Tritium Science Program FY24 Report:

First-Principles Studies of Tritium Species Diffusivity Across the Interface of Nickel-Plated Zircaloy-4

Hari P. Paudel[1,2], De Nyago Tafen[3,4] and Yuhua Duan[1*]

[1]U.S. Department of Energy, National Energy Technology Laboratory, 626 Cochran Mill Road, Pittsburgh, PA 15236-0940, USA

[2]NETL Support Contractor, 626 Cochran Mill Road, Pittsburgh, PA 15236-0940, USA

[3]U.S. Department of Energy, National Energy Technology Laboratory, 1450 Queen Avenue SW, Albany, OR 97321 USA

[4]NETL Support Contractor, 1450 Queen Avenue SW, Albany, OR 97321 USA

DOE/NETL-2025/4904 October 30, 2024

DISCLAIMER

Table of Contents

List of Figures

1 INTODUCTION

1.1 Background

Enhancing tritium production in nuclear reactor requires optimal and consistent performance of materials that are integrated in tritium producing burnable absorber rod (TPBAR). Materials that are used within TPBAR usually have excellent physical and chemical properties and are corrosion resistant under highly energetic radiation combined with pressurized water, high pressure, and temperature. Zirconium (Zr) and its alloys are materials widely used in nuclear reactors as ^{3}H getters due to their low absorption cross-section of thermal neutrons, good mechanical, and thermal properties. In addition, their excellent mechanical and thermal properties, Zr and its alloys are considered as best getter materials over refractory alloys such as stainless steel. Under energetic neutron irradiation in pressurized water reactor (PWR), the lithium aluminate pellets produce ^{3}H which diffuses to the getter materials by passing through a thin layer of Nickel. A chemical reaction between ^{3}H and Zr yields metal hydride ($Zr^{3}H_{x}$), precipitation of which results in overall increase of volume and embrittlement of alloys.[1] This adversely affects the performance and life span of Zr alloy used as a getter. The computational study using a realistic model can provide better understanding of ^{3}H diffusion mechanisms and chemical reaction that results metal hydride formation as fuel burn-up increases in zircalloy.

We conducted a series of studies on γ-$LiAlO_2$ and Li_2ZrO_3 pellets to understand the formation of tritium species and their diffusion in the pellets [2, 3]. We studied the surface properties, diffusion of ^{3}H and $O^{3}H$ species in defective (100) and (101) surfaces, and the $^{3}H_2O$ formation, its adsorption and desorption process in γ-$LiAlO_2$ and $LiAl_5O_8$ surfaces [4, 5]. We found that release of ^{3}H depends on number of Li vacancies, initially ^{3}H is being main product and as Li vacancy increases $^{3}H_2$ could also be released.

We investigated ^3H diffusion in different zirconium hydrides [1, 6, 7]. However, there remain open questions that need the answers: (i) how does ^3H diffuse into Ni/zircaloy-4 interface? and (ii) how does the impurities such as Sn and O impact the diffusion of 3H across the Ni/zircaloy-4 interface?

The species such $^3H_2$ and ^3H_2O that are generated at the γ-$LiAlO_2$ pellets [4, 5] are usually diffuse to the Ni-plated Zircaloy-4 getters through the vacuum space in between the Ni and the pallet. The species are captured by Zr after they diffuse through Ni coating forming the Zr hydride. In FY2023, we conducted detail investigation on $^3H_2$ and ^3H_2O binding sites and their dissociation on the (111) surface of Ni.[8] We concluded that the possible dissociation steps were $^3H_2O \rightarrow O^3H + {}^3H \rightarrow O + {}^3H + {}^3H$, and $^3H_2 \rightarrow {}^3H + {}^3H$. The relative energies of ^3H binding sites on Zr(001) and Zr(100) were also determined. Detail investigation was conducted on the ^3H diffusion on the surface and subsurface region of Zr. The effect of Sn on ^3H was shown to have a strong repulsive effect.[1, 7] Several possible paths were proposed for surface to bulk diffusion mechanisms. In FY2024, based on the interface model of Ni-Zircaloy-4 that we produced in FY23, we further explored the diffusion pathways of ^3H across the interfaces under different conditions, including with oxide/hydroxide clusters on Ni layer, impurities (e.g. Sn, and O) at the interface region.

1.2 Project Technical Scope

The Zr alloys used in TPBARs are pure and can almost be chemically regarded as single-component systems. The Zricaloy-4 with small alloying elements of Sn (< 2%) and Fe (< 1%) in Zr metal has been used to build the interface model of Ni and Zircaloy-4 in our calculations. The impurities (Sn, and O) were introduced in the simulation model. To explore the ^3H species diffusion with impurities across the interface and dissolution into the Zircaloy-4 getter, a Ni-Zr interface model was constructed by matching 9x9 (or 5x5) Ni (111) and 7x7 (or 4x4) Zr (0001) surfaces with an optimized interface distance ($d_z \approx 2.3$ Å).[8] We explored the ^3H diffusion from Ni side to Zr side, where ^3H chemically reacted to form metal hydrides. We introduced the $NiO_x/Ni(OH)_x$ on Ni side and Sn and C impurities with vacancies on the Zr side at the interface region. The Ni(111)-Zr(0001) models with different number of layers were optimized with

respect to the bond length across the interface. The diffusion barriers for ^{3}H with and without impurities, and defects were predicted.

To achieve our objectives, we conducted the investigation by using spin-polarized density functional theory (DFT) methods. The employed method captured the magnetic features of Ni and its impact on the ^{3}H diffusion. The proposed study used the NETL's supercomputer facility. This project was divided into three subtasks:

- **Task 1**: *Exploring ^{3}H diffusion across pure Ni-Zr interface*. The diffusion pathway will be obtained and serves as our baseline for the following tasks.
- **Task 2**: *Calculating the ^{3}H diffusion pathways across the Ni-Zr interface when $NiO_x/Ni(OH)_x$ appeared in the Ni side of the interface region*. Based on the pure Ni-Zr interface model from Task 1, we will introduce $NiO_x/Ni(OH)_x$ clusters on the Ni side closer to the interface. Then, the ^{3}H diffusion pathways and barriers from Ni side to the zircalory-4 will be explored. We will investigate how $NiO_x/Ni(OH)_x$ affects the ^{3}H diffusion across the interface.
- **Task 3**: *Exploring the effects of impurities on ^{3}H diffusion in Ni-plated Zircaloy-4 getter*. Based on the model constructed in Task 2, we will introduce impurities (e.g. Sn, Fe, C, defects) on the Zr side of the interface. Then, the pathways and barriers of ^{3}H diffusion from Ni side to the zircalory-4 will be calculated. From this task, we will determine whether the impurity can help or hinder the ^{3}H diffusion into Zircalory-4 getter to form $Zr^{3}H_x$ phases for ^{3}H storage.

1.3 Deliverables

In FY2021, we published following peer reviewed papers and made presentations from this project:

Publications

- H. P. Paudel, T. Jia, W. A. Saidi, D. J. Senor, A. M. Casella, Y. Duan, "*Study of Tritium Diffusivity in Pure and Sn Defective Zr: A First Principles Density Functional Theory Approach*", **J. Phys. Chem. C 127**(26)(2023)12435-12443. doi: 10.1021/acs.jpcc.3c01200.
- D. N. Tafen, H. P. Paudel, D. J. Senor, A. M. Casella, Y. Duan, "*Solubility and Diffusivity of Tritium Species in Interface of Nickel-Plated Zircaloy-4: First Principles Density Functional Study*", **Phys. Chem. Chem. Phys**. **27**(2025)481-489. doi:10.1039/d4cp04398g.
- M. Redington, H. P. Paudel, D. N. Tafen, Y. Duan, "*Tritium Adsorption on Surfaces of Pure and Tin-Defective Zirconium*", **Journal of Physical Chemistry C** under review (2024).
- H. P. Paudel, D. N. Tafen, Y. Duan, *Tritium Diffusion Across the Interface of Nickel-Plated Zircaloy-4: A First Principles Density Functional Theory Study*, Under preparation (2024).

Presentations

- Y. Duan, H. Paudel, D. N. Tafen, T. Jia, D. Senor, A. M. Casella, "*First-principles study of the tritium formation in γ-$LiAlO_2$ pellets and diffusion into Zircaloy-4 getter*", **APS March Meeting**, Mar.03-08, 2024, Minneapolis, MN
- H. P. Paudel, D. N. Tafen, Y. Duan, "*First-Principles Studies of Tritium Species Diffusivity Across the Interface of Nickel-Plated Zircaloy-4*", 9th **Annual Tritium Science Technical Exchange**, September 17-18, 2024, Pacific Northwest National Laboratory, Richland, WA.

1.4 Organization of Report

We organize this report as follow. We present theoretical and computational methodologies implemented in this work in the chapter 2. We present and discuss the results of our study for 3H diffusion mechanisms in the chapter 3. We systematically present our investigation on creating Ni and Zr surfaces, interfaces, and diffusion energy barriers with and without Zr vacancy, Sn and O impurities in the interface. Diffusion property calculations is based on the interface made of Ni(111) and Zr(0001) surfaces with five

layers. We also created and optimized Ni(111)-Zr(0001) interface consisting of six- layers. We summarize our study and present the outlook in chapter 4.

2 THEORITICAL AND COMPUTATIONAL METHOD

2.1 Background

α -Zr and its alloys are materials used in nuclear reactors as ^{3}H getter. Ni is coating helps to screen moisture by dissociating water. O_2 molecule has several times higher diffusion barriers in Ni than ^{3}H, making O species harder to diffuse to the zircaloy-4 getter.[9] Getters are exposed to high radiation and extremely corrosive environments[10]. The ^{3}H produced at pallet diffuses through the Ni-Zr interface. While the modelling of the Ni-Zr interface is challenging due low symmetry sites, changes in atomic positions and intermixing of atoms at the interface region, a simple slab model could provide insight on the interface geometry, ^{3}H solubility and diffusivity across the interface. Computationally, this task could be further challenging at the DFT level of calculations due to low symmetry sites of impurity and defects. In this chapter, we will provide our computational and theoretical details about the approach for the study of interface models, solubility, and diffusivity for ^{3}H with and without vacancy defects, Sn and O impurities at the interface region.

2.2 Computational Method

The calculation were performed using the density functional theory (DFT) approach with the plane-wave basis set as implemented in the Vienna ab initio simulation package (VASP) [11]. The electron-ion interaction is described with the projector augmented wave method (PAW) [12]. The potential of the isotope ^{3}H was obtained by modifying the mass in the standard ^{1}H potential. The exchange and correction interactions were described within generalized gradient approximation using the spin-polarized Perdew-

Burke-Ernzerhof formulation (GGA-PBE) [13]. The convergence in energy was achieved using a cutoff energy of 400 eV for the plane wave expansion. The convergence was optimized with change in total energy and force until 10^{-5} eV and 0.01 eV/Å, respectively were achieved.

We used Zr(0001) in a form of slab of 100 atoms, and corresponding to four layers of 25 atoms. In our previous work (under press) calculations on Zr(100) was also performed with a slab of 90 atoms, that had six layers of 15 atoms.[14] Each surface system had a vacuum space of 20.0 Å fixed along the z-axis to avoid the interaction between periodic images. For Ni systems with varying slab's size and number of atomic layers were generated from the fully relaxed bulk structure. For the Ni (111) surfaces we used a three-layered 5 × 5 supercell slab with a vacuum region of 12 Å along the z-axis. The k-point sampling in a reciprocal space was generated using Monkhorst-Pack method and a 3 × 3 × 1 grid size. We created an interface by using Ni(111) and Zr(0001). The interface was optimized and the bond distances between Ni and Zr were calculated. We introduced ^{3}H at the interface region and calculated its formation energy. The diffusion barriers were calculated for ^{3}H with and without Zr vacancy, Sn and O impurities. The nudge elastic band (c-NEB) approach was implemented to calculate the diffusion barriers. [15] More than five images were used for each diffusion pathways to map the potentials barriers.

3 RESULTS AND DISCUSSION

3.1 Introduction

In order to model Ni-Zr interface, first we need to optimized individual surface and then interface these surfaces. The interface is further optimized to create a most stable geometry, which can be further used to calculate the 3H solubility and diffusivity. In the past, by using optimized bulk Zr structure, we created Zr(0001) surface with varying number of layers and further optimized by minimizing the surface energies.[14] The formation energies for ^{3}H was calculated on Zr(0001) surfaces.[14] The surface-to-surface

diffusion barriers for ^3H on these surfaces were calculated. The effect of Sn on ^3H was shown to have a strong repulsive effect on these surfaces. Several possible paths for surface to bulk diffusion were proposed. We showed that results reproduced both the dissociation of $^3H_2$ on Zr and previously calculated energy profiles for the transfer of ^3H in bulk Zr. Surface to subsurface diffusion was found to have similar to that of ^3H with Sn on the surface of the pristine Zr surface. The diffusion from a pristine surface to a Sn doped subsurface was found to have a significant energy barrier for both the forward and reverse reaction processes. This showed that Sn in the subsurface region hindered the desorption of ^3H. In our previous study for ZrH system, we also predicted that as the ^3H concentration increased from x = 0.5 to x = 2, the calculated energy barriers to be 0.31, 0.38, 0.73, and 1.48 eV for $ZrT_{0.5}$, ZrT, $ZrT_{1.5}$, and ZrT_2, respectively.[4, 6] The presence of Sn impurity was found to increase those barriers due to slightly prelusive nature of the Sn-H interaction. Also, our study from FY2023 indicated that O is most likely stay in the Ni layer to form NiO_x or $Ni(O^3H)_x$ and formation of these NiO species is limited by O diffusion energy barrier and availability of the Ni vacancy. Here we provide detail investigation of ^3H diffusion mechanisms across the Ni-Zr interface without and with Sn and O impurity in Ni and Zr region.

3.2 Modelling of Ni-Zr Interfaces

Surface modelling is a crucial part of constructing and designing an interface. In the past we modeled Ni(111) and Zr(0001) surfaces and optimized for the 3H diffusion on the surface and subsurface region. We modeled the interface with Ni(111) surfaces consisting three and four layers in order to capture the effects coming from using different number of layers. The bond length for Ni is; $a_{Ni} = 2.475$ Å, and bond length for Zr is; a_{Zr} = 3.17 Å. Most of the time the stability of the interface is severely hampered if there is huge lattice parameter mismatch between two different materials forming the interface. Ideally, we require the bond length ratio in xy plane is; a_{Zr}/a_{Ni} ~1 so that atoms are subjected under minimal stressed environment at the interface region and retain maximum symmetry of the lattice sites. With 5×5 surface of Ni(111) and 4×4 surface of Zr(0001), the bond length ratio; a_{Zr}/a_{Ni}~1.032. Next best match in the

lattice parameter is obtained with 9×9 surface of Ni(111) and 7×7 surface of Zr(0001). These surfaces yield the bond length ratio closer to unity, but the size of the interface and the number of atoms is beyond the computational capabilities for DFT. The calculation of diffusion dynamics for larger interface model demands high computational resources even though the optimization of the model itself is doable if ions are freeze while optimizing the structure.

3.2.1 Ni(111)-Zr(0001) Interface Optimization

We modelled Ni(111)-Zr(0001) interface that consisted of two layers of Ni and three layers of Zr surfaces. Optimized 5×5 surfaces of Ni(111) and 4×4 surface of Z(0001) were constructed from their respective bulk using Material Studios program. The two surfaces were interfaced, and boundary atoms were realigned and edited in order to best match the interface region. The interface was perpendicular to the crystallographic $c-$axis. The constructed interface was computationally optimized. We constructed two interfaces each with total of five and six layers as shown in Figure 1. We calculated the Ni-Zr bond length over the ranges of two Å and optimized the structure. Figure 3 a and b show an interface model with total of five layers and model optimization by varying the bond length. The bond length of $d_z = 2.32$ Å was found corresponding to minimum total energy for the five-layer system. The minimum Ni-Zr bond length was found to be $d_z = 2.35$ Å for the six-layer interface. On the Ni side, Ni-Ni bond was found to vary between 2.50 to 2.65 Å. The atoms were more displaced along $c-$axis and minimally displaced along $a-$axis. Similarly, atoms were displaced more than by an Å in the boundary of Zr slab. These models will be further used to calculate the diffusion energy barriers.

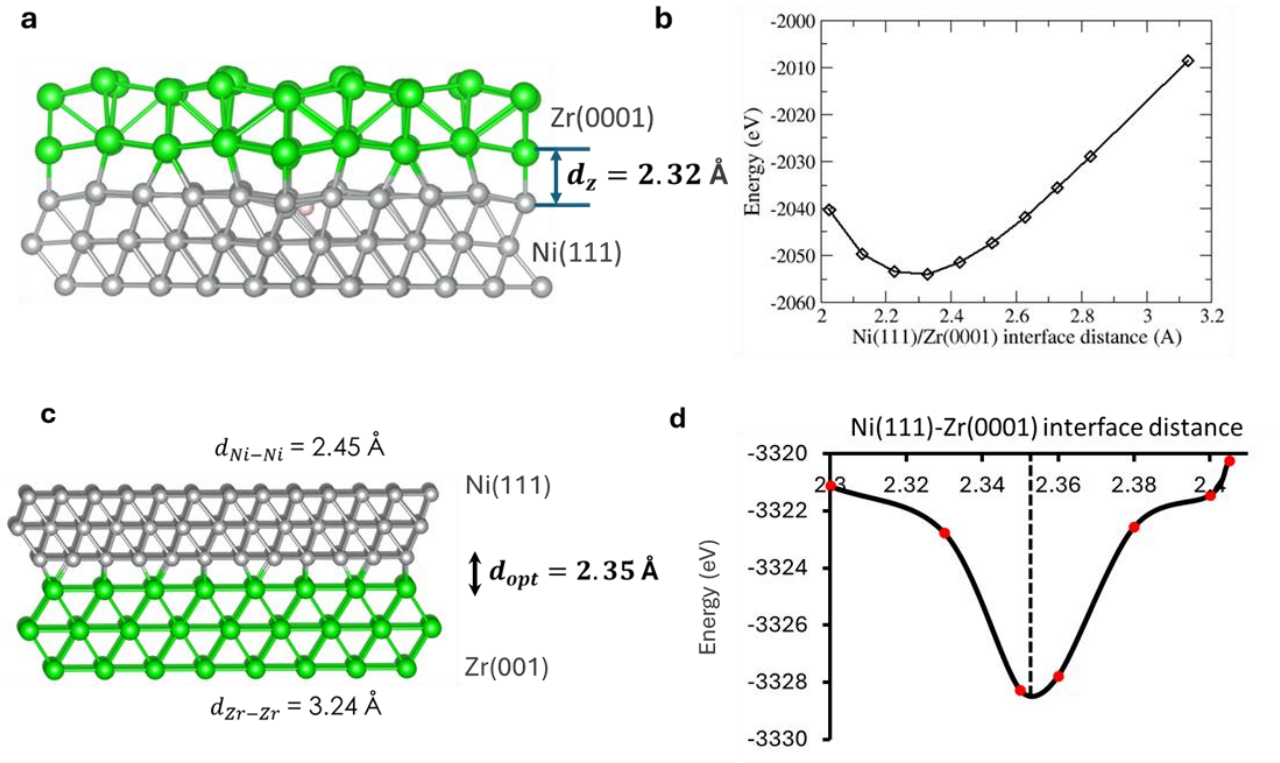

Figure 1: Ni(111)-Zr(0001) interface with five layer model and energy optimization (a, b) and with six layers model (c, d). The bond length was optimized by minimizing the total energy. The interface was perpendicular to the crystallography $\boldsymbol{c}$ −axis. color codes- grey: Ni, green: Zr, pink: ^{3}H.

3.3 ^{3}H Formation and Diffusion Across Ni-Zr Interface

3.3.1 Vacancy and Impurity Formation

Vacancy defects in the Zr side of the interface can be modeled by taking a Zr (0001) surface model and removing an atom from near the interface region. The system with a vacancy was then optimized, and the vacancy formation energy E_{vac} was calculated using,

$$E_{vac} = E - NE_{surf} \qquad 3\text{-}1$$

where E is the total energy of the optimized system with the defect and N is the number of atoms. E_{surf} is the total energy of the interface with no vacancy defect. The interstitial formation energies were calculated using,

$$E_f = E - (N+1)\, E_{surf} \qquad 3\text{-}2$$

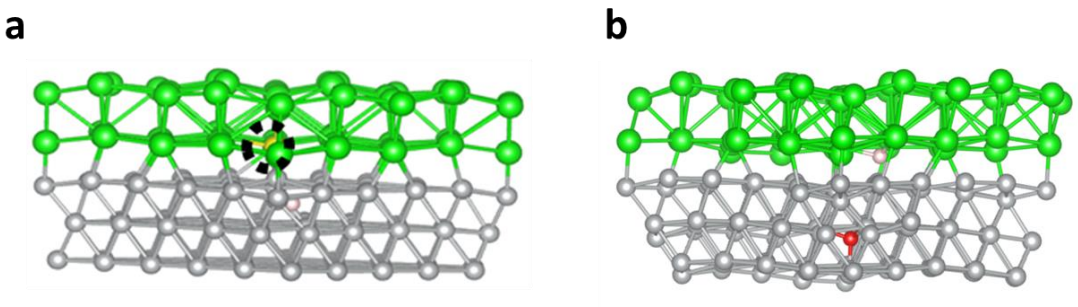

Figure 2: A Zr vacancy in Zr side of the interface (a), and formation of Ni(OH) near the interface (b). color codes- grey: Ni, green: Zr, pink: ^{3}H, yellow: Zr vacancy, red: O

while interfacing optimized Zr (0001) and Ni (111) surfaces, the new geometry in the optimized structure has very low symmetry due to not perfect alignment of the lattice parameters. Due to low symmetry, the formation energy of the vacancies and impurities are expected to drastically alter at the interface region than pure slab systems. We introduced a Zr vacancy, and ^{3}H and O impurities in interface Ni(111)/Zr(0001) as shown in the Figure 1. The formation of O and H in the Ni(111) side in the interface model could form a complex compounds such as $Ni_xO_yH_z$. The formation energy of such compounds can be defined as follows:

$$\Delta H\left(Ni_x O_y H_z\right) = E_{DFT}\left(Ni_x O_y H_z\right) - x\mu_{Ni}^{solid} - y\mu_O^{gas} - z\mu_H^{gas} \qquad 3\text{-}3$$

where $E_{DFT}\left(Ni_x O_y H_z\right)$ is the DFT calculated total energy of the compound; μ_{Ni}^{solid}, μ_O^{gas}, and μ_H^{gas} are the chemical potentials of Ni, O, and H in the stable elemental solid/gas state; x, y, z are the respective concentrations. In FY2023, we calculated the total and formation energies of the most stable compounds of nickel oxides and hydroxides by using different exchange correlation functionals in DFT calculations. [8] Our results from the last year were good in agreement with the experimental data. [16]

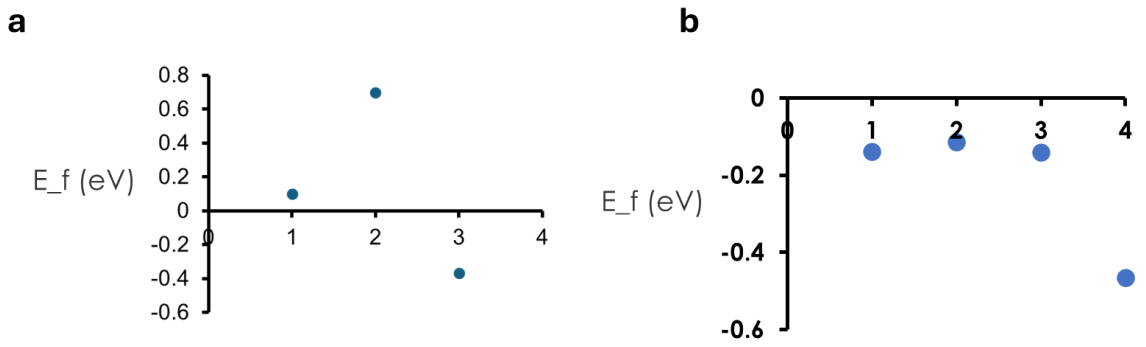

Figure 3: ^{3}H formation energy in Ni side and Zr side (b) of the interface Ni(111)-Zr(0001).

To get most stable site for ^{3}H in Ni and Zr side of the interface, we optimized the structures and calculated the formation energy. We introduced ^{3}H in the intertrial sites of the Zr. Due to a low-level symmetry across the interface region, there could be a number of local minima where ^{3}H could be transiently trapped. Figure 3 a and b shows the few sites with the corresponding formation energies for ^{3}H both sides of the interface. The lowest ^{3}H formation energy in the Ni site was found to be -0.36 eV closer to the Zr atom. ^{3}H in some other sites such as top and distorted tetrahedra sites in Ni gives positive formation energy. Similarly, the lowest ^{3}H formation energy in Zr site was found to be -0.46 eV among several sites we optimized in our calculations. These values are different from ^{3}H formation energies in the pure Ni and Zr bulk as the symmetry is highly reduced while sandwiching two surfaces.

3.3.2 ^{3}H Diffusion in Pure and Zr Vacancy Defective Interface

We continued with the interfaces in Figure 3 and ^{3}H optimized structure to investigate the diffusion mechanisms for ^{3}H with and without Zr vacancy across the interface. As discussed earlier in this report, ^{3}H was introduced in the Ni tetrahedral interstitial site. The initial and final states of ^{3}H in the Ni(111)-Zr(0001) interface are shown in Figure 4 a and b. In the FY2023 work, we thoroughly discussed about the formation of ^{3}H in the surface and Ni and we had a number of investigations for stability of ^{3}H in surface

and bulk Zr.[8] After identifying the initial and final states of ^{3}H, we mapped the migration pathways by using eight images as shown in Figure 4 c.

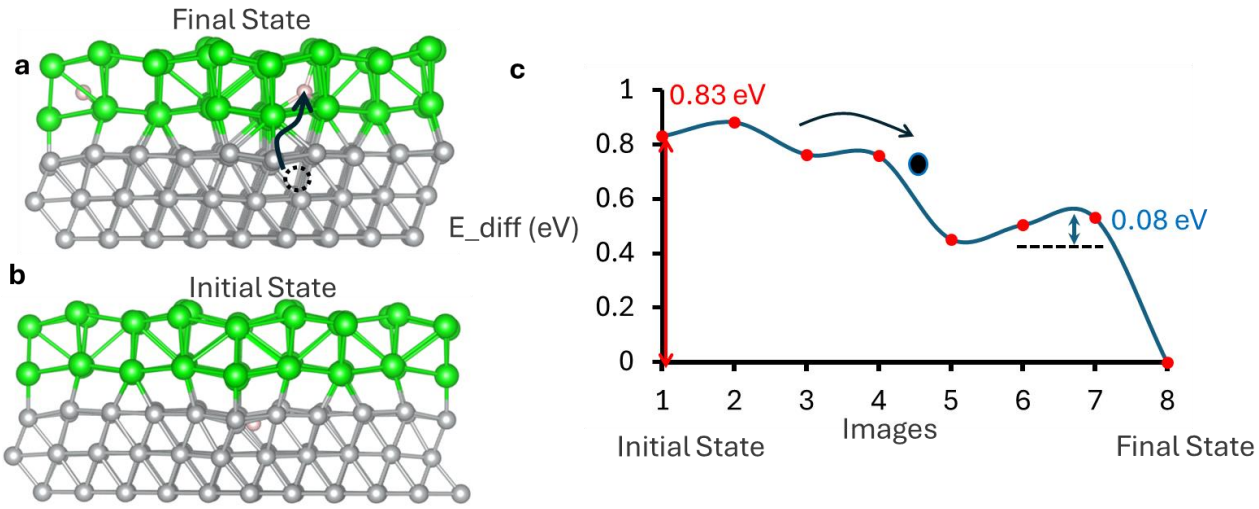

Figure 4: Final (a) and initial (b) state of ^{3}H. There is no overall diffusion barrier for ^{3}H while diffusing from Ni to Zr side as shown in figure (c). The final state is more stable by 0.83 eV.

In the metal, ^{3}H usually forms a week bond. The ^{3}H bonding in Ni is weaker than in the ^{3}H bonding in Zr. ^{3}H chemically reacts with Zr to form hydride phases. The initial state at Ni was found to be 0.83 eV higher than the final state. Due to corrugated potentials along the interface region, the potential energy profile was found to have several local minima. Since there was no barrier for ^{3}H, it was found that as ^{3}H arrives at Ni, it spontaneously diffuses to Zr to form ZrH_x.

In order to calculate the impact of Zr vacancy on ^{3}H diffusion, we created a Zr vacancy near the interface near the pathway calculated in Figure 4. Figure 5 shows the diffusion barrier profile for ^{3}H across the interface in presence of Zr vacancy. The initial state was found to be less stable by 0.74 eV than the final state. This energy difference was 0.1 eV less than when there was no Zr vacancy.

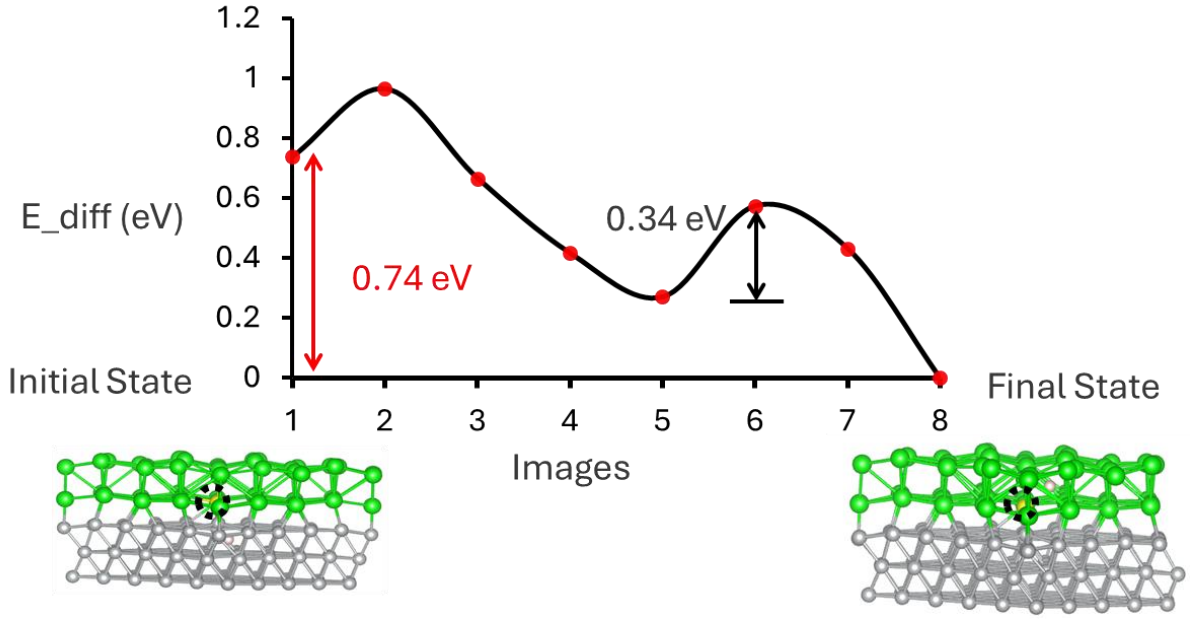

Figure 5: Diffusion energy barrier for ^{3}H in presence of Zr vacancy. The dotted circle indicates the Zr vacancy site.

3.3.3 ^{3}H Diffusion with Sn and O Impurities

In this section, we provide description on diffusion mechanisms, pathways, and migration profiles in presence of Sn and O impurities in the interface model. We introduced a substitutional Sn impurity in Zr side as shown in Figure 6. The initial state was found to be 0.24 eV less stable than the final state. Initially, ^{3}H sees a barrier of 0.3 eV which falls rapidly for the site right at the interface. At the interface, it was found that the diffusion barrier was negative with trapping well of -0.2 eV as shown by vertical dotted lines in Figure 6. This indicated that ^{3}H could be transiently trapped near the interface. After the trapping well, the barrier was found to be 0.75 eV. The atoms sites at the interface are displaced which reduces the symmetry. The displacement of atoms alters the potential profiles, eventually creating such wells along the interface.

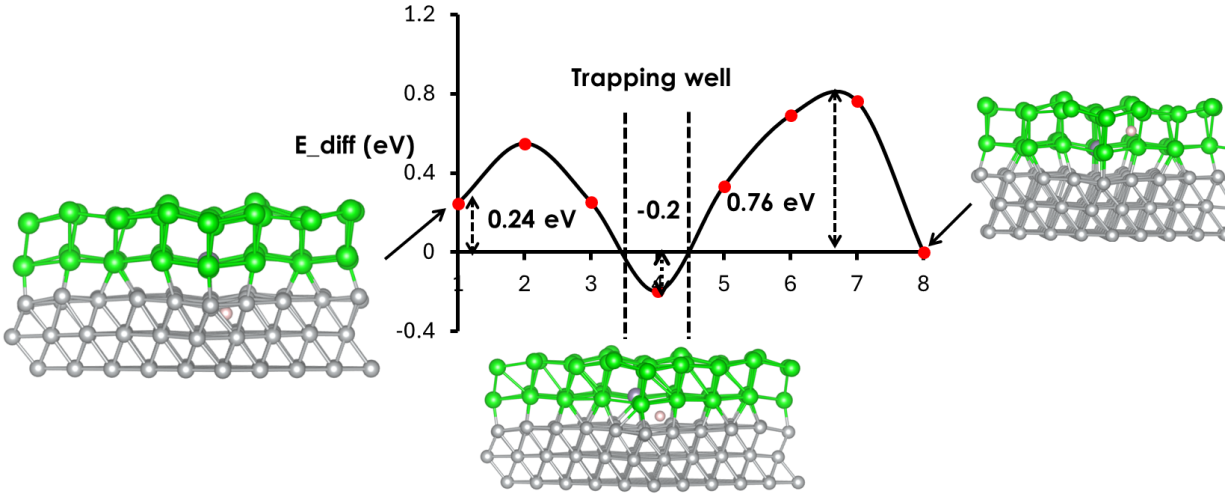

Figure 6: Diffusion barrier for ^3H in presence of Sn in Ni(111)-Zr(0001) interface. The region between two vertical lines is a trapping well, where ^3H could be transiently trapped.

The presence of O in Ni creates an oxide phase. In FY2023, we studied the formation and stability of several NiO_x species. In that study, we found that there exists a stable chemical potential region where NiO_x or $Ni(O^3H)_x$ phase are formed and $^3H_2$ dissociates on the surface of Ni and diffuses into the subsurface. We also predicted that formation of NiO_x or $Ni(O^3H)_x$ phase in Ni subsurface layer is limited by O diffusion energy barrier and Ni vacancy. To better understand the effect of O impurities and NiO formation on the diffusion barrier for ^3H, we introduced O in the interstitial site within Ni. We identified the most stable site for O and ^3H, by calculating the formation energy of the O^3H, entity as shown in Figure 7. Calculation for the formation energy showed that the O and ^3H, cannot form a bound entity such O^3H, in Ni. The energy for O^3H formation was highest when they were apart to each other. The highest formation energy found for the cases we calculated was -6.59 eV as shown in Figure 7. Using the most probable site for O^3H, next we begin to investigate the diffusion mechanism in presence of O and its impact on the diffusion barrier.

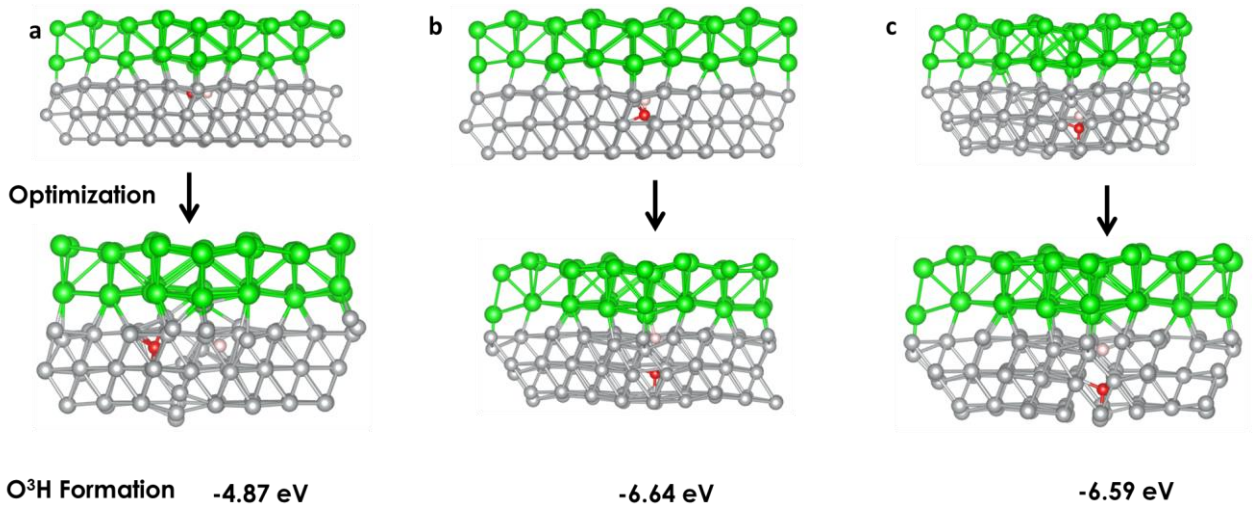

Figure 7: Ni(OH) optimization in Ni(111)-Zr(0001) interface, upper row for before the optimization and lower row after the optimization with O and ^{3}H at different sites.

To calculate the diffusion energy barrier with O, we repeated the migration pathways for ^{3}H and evaluated the impact of O on the diffusion energy profile. Figure 8 shows the diffusion energy barrier and the initial, transition and final states for ^{3}H. Initial energy barrier for ^{3}H diffusion in the interface was found to be 0.35 eV, almost 0.25 eV higher than without O impurity. ^{3}H is more stable by 0.43 eV in Zr region than in the Ni region. The barrier 0.35 eV was found in between Ni and Zr site as indicated by the transition state in Figure 8. The calculated pathways of diffusion for ^{3}H showed that the O and ^{3}H may have local minimum sites separated by more than 1 Å. The above value for diffusion barrier was comparable to our previously barrier energy of 0.23 eV in Zr^{3}H with low concentration of ^{3}H for tetrahedral-to-tetrahedral site diffusion.[1, 2, 6, 7]

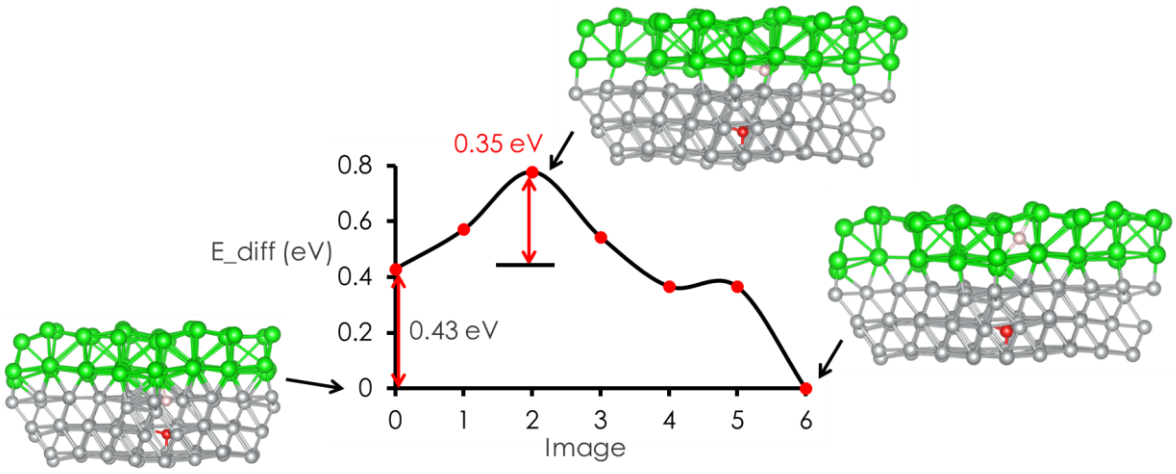

Figure 8: Diffusion barrier for ^{3}H in presence of O impurity. Initial energy barrier for ^{3}H diffusion in presence of O at the interface was found to be 0.35 eV, almost 0.25 eV higher than without O impurity. ^{3}H is more stable by 0.43 eV in Zr region.

We also investigated the diffusion mechanisms with Sn and O impurities in the interface system. A substitutional Sn impurity was optimized in the structure with already presented O impurity. It was found that the Sn is most stable when replaced to one of the Zr atoms making Ni-Zr bond as shown in the inset in Figure 9. In this case, the final state was found to be more stable by 0.15 eV than the initial state, which indicated that ^{3}H is still more stable at Ni lattice site than at Zr. The relative stability for ^{3}H was found to decrease in impure interface as compared to the pure interface (Figure 4.) We calculated the barrier energy of 0.15 eV with Sn and O impurity as shown in Figure 9. At the peak of the barrier, the transition state has Sn-^{3}H bond length of 2.15 Å, which is higher than Sn-^{3}H bond at the final state.

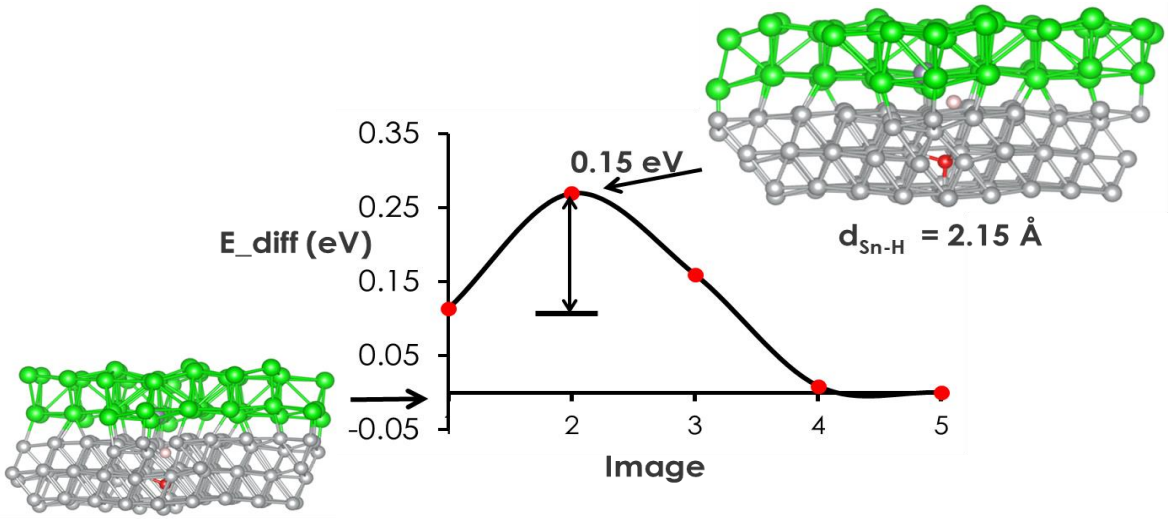

Figure 9: Diffusion barrier for ^3H in presence of O, and Sn in Ni(111)-Zr(0001) interface.

4 SUMMARY OF REPORT AND FURTHER WORK

α-Zr and its alloys are known as best ^3H getters due to their excellent corrosion resistance under chemically corrosive environment, low thermal neutron absorption cross-section and robust mechanical strength at high temperature. In TPBAR, chemical corrosion rate is further enhanced due to high temperatures and radiation carrying MeV of energy. α-Zr and its alloys such as zircaloy demonstrate excellent physical and chemical properties that allow high ^3H retention rate and low overall material failure probability. In TPBAR, zircaloy as a getter is interfaced with thin layer of Ni in order to stop chemical species such O_2 and allows ^3H freely diffuse to the getter. Our FY2023 study revealed that ^3H has several times smaller energy barrier to diffuse to the interface as compared to O and O^3H in Ni(111) surface. Ni metal has low binding energy for ^3H and so it forms loosely in Ni surface. The molecule such as ^3H_2O was found to be disassociated on the Ni surface. Understanding of diffusion mechanisms of ^3H across the Ni-Zr interface provides insight on the structure of interface and its better design for higher retention of ^3H.

In FY2024, we conducted a systematic study on constructing and optimizing Ni and Zr surfaces, interfacing the stable Ni and Zr surfaces to create an optimal Ni-Zr interface and an understanding the diffusion mechanisms for ^{3}H with and without vacancies and impurities such as Sn and O. We optimized a Zr(0001) surface from the bulk Zr, and found stable Zr vacancy and interstitial ^{3}H formation site. We also optimized the Ni(111) surface and identified ^{3}H formation site. We created an interface of Ni(111)-Zr(0001). We further optimized the interface energy with respect to Ni-Zr bond length. We found optimized Ni-Zr bond lengths were 2.32 Å and 2.35 Å, respectively for the five- and six- layer systems. We introduced interstitial ^{3}H in the Ni side of the interface. The diffusion energy barrier was found to be downhill going from Ni to Zr. The relative energy difference was found to be more than 0.8 eV. This indicated that ^{3}H loosely bound at Ni and it spontaneously diffuses to the Zr side to form $Zr^{3}H$. We created a Zr vacancy and investigated the impact to the diffusion barrier. The relative energy difference between initial and final state was found to decrease by 0.1 eV as compared to without a vacancy, and a barrier of 0.34 eV was calculated. Next, we introduced interstitial Sn impurity in the ^{3}H diffusion pathways. In this case, we found that 3H is more stable in Zr region than Ni by 0.24 eV. Near the Ni-Zr bonding sites, ^{3}H was found to have a trapping well of energy height -0.2 eV. We then introduced O in the Ni side of the interface. A diffusion barrier of 0.15 eV was calculated with Sn and O impurities. ^{3}H was found to be more stable by 0.11 eV on the Zr side than in Ni. This relative stability was less by more than 0.3 eV when with only O impurity. Form our study, we conclude that a) ^{3}H spontaneously diffuses to Zr from Ni with no or very small interface barrier and b) Impurities such as Sn in Zr and O in Ni reduce the relative stability of ^{3}H in Zr.

Larger Ni-Zr interface models with larger number atoms are computationally challenging for diffusion properties calculation. We also constructed Ni(001)-Zr(0001) interface model, where each surface had four layers, making total of eight layers in the interface system. This was already challenging to implement for the diffusion energy barrier calculations. Our preliminary study indicates that the Ni atoms are

diffusing to the Zr side at the interface region.[17] In the past, CALPHAD modelling was used to assess the different possible phases of Ni_xZr_y at the interface region.[18] A detail understanding of the Ni diffusion in Zr subsurface and its impact on the diffusion for ^3H is still lacking. The future study would be worth conducting on studying the Ni mixed Ni-Zr interface and diffusion mechanisms for ^3H, and comparing those calculated properties for the mixed interface with the pure interface systems.

5 ACKNOWLEDGEMENTS

This research is supported by the National Nuclear Security Administration (NNSA) of the U. S. Department of Energy (DOE) through the Tritium Modernization Program. We thank the National Energy Technology Laboratory (NETL) Research and Innovation Center providing Computational resources. We thank the Tritium Science Program Manager, Drs. David Senor and Andrew M. Casella (PNNL), for their excellent managemental skills and helpful comments on this work.

This research was also supported in part by an appointment with the AMMTO Summer Internships program sponsored by the U.S. Department of Energy (DOE), EERE Advanced Materials and Manufacturing Technologies Office (AMMTO). This program is administered by the Oak Ridge Institute for Science and Education (ORISE) for DOE. ORISE is managed by ORAU.

constitute or imply its endorsement, recommendation, or favoring by the United States Government or any agency thereof. The views and opinions of authors expressed herein do not necessarily state or reflect those of the United States Government or any agency thereof.

6 REFERENCES

(1) Andolina, C. M.; Saidi, W. A.; Paudel, H. P.; Senor, D. J.; Duan, Y. Hydrogen localization and cluster formation in α-Zr from first-principles investigations. *Computational Materials Science* **2022**, *209*, 111384. DOI: https://doi.org/10.1016/j.commatsci.2022.111384.

(2) Paudel, H. P.; Duan, Y. A First-Principles Density Function Theory Study of Tritium Diffusion in Li2ZrO3: Application for Producing Tritium. *The Journal of Physical Chemistry C* **2018**, *122* (50), 28447-28459. DOI: 10.1021/acs.jpcc.8b05810.

(3) Paudel, H. P.; Lee, Y.-L.; Senor, D. J.; Duan, Y. Tritium Diffusion Pathways in γ-LiAlO2 Pellets Used in TPBAR: A First-Principles Density Functional Theory Investigation. *The Journal of Physical Chemistry C* **2018**, *122* (18), 9755-9765. DOI: 10.1021/acs.jpcc.8b01108. Lee, Y.-L.; Holber, J.; Paudel, H. P.; Sorescu, D. C.; Senor, D. J.; Duan, Y. Density functional theory study of the point defect energetics in γ-LiAlO2, Li2ZrO3 and Li2TiO3 materials. *Journal of Nuclear Materials* **2018**, *511*, 375-389. DOI: https://doi.org/10.1016/j.jnucmat.2018.09.030. Duan, Y.; Sorescu, D. C.; Jiang, W.; Senor, D. J. Theoretical study of the electronic, thermodynamic, and thermo-conductive properties of γ-LiAlO2 with 6Li isotope substitutions for tritium production. *Journal of Nuclear Materials* **2020**, *530*, 151963. DOI: https://doi.org/10.1016/j.jnucmat.2019.151963.

(4) Jia, T.; Senor, D. J.; Duan, Y. First-principles study of the tritium reaction and diffusion on the γ-LiAlO2 (1 0 0) surface with carbon impurity. *Computational Materials Science* **2020**, *181*, 109748. DOI: https://doi.org/10.1016/j.commatsci.2020.109748.

(5) Jia, T.; Senor, D. J.; Duan, Y. Tritium species diffusion on and desorption from γ-LiAlO2 (100) surface: A first-principles investigation. *Journal of Nuclear Materials* **2020**, *540*, 152394. DOI: https://doi.org/10.1016/j.jnucmat.2020.152394. Jia, T.; Senor, D. J.; Duan, Y. Trapping and recombination of tritium in lithium vacancy of the γ-LiAlO2 (100) surface: A first-principles study. *Applied Surface Science Advances* **2021**, *5*, 100114. DOI: https://doi.org/10.1016/j.apsadv.2021.100114. Jia, T.; Senor, D. J.; Duan, Y. First-principles study of the surface properties of LiAl5O8: Stability and tritiated water formation. *Journal of Nuclear Materials* **2021**, *555*, 153111. DOI: https://doi.org/10.1016/j.jnucmat.2021.153111. Jia, T.; Zeng, Z.; Paudel, H.; Senor, D. J.; Duan, Y. First-principles study of the surface properties of γ-LiAlO2: Stability and tritium adsorption. *Journal of Nuclear Materials* **2019**, *522*, 1-10. DOI: https://doi.org/10.1016/j.jnucmat.2019.05.007. Paudel, H. P.; Senor, D. J.; Duan, Y. Effects of carbon impurity on tritium diffusion and helium formation in γ-LiAlO2 pellets: A first-principles study. *Computational Materials Science* **2021**, *193*, 110419. DOI: https://doi.org/10.1016/j.commatsci.2021.110419.

(6) Jia, T.; Paudel, H. P.; Senor, D. J.; Duan, Y. First-principles studies of the concentration-dependent tritium diffusion in the zirconium hydrides with and without Sn impurity. *Computational Materials Science* **2022**, *203*, 111158. DOI: https://doi.org/10.1016/j.commatsci.2021.111158.

(7) Paudel, H. P.; Jia, T.; Saidi, W. A.; Senor, D. J.; Casella, A. M.; Duan, Y. Study of Tritium Diffusivity in Pure and Sn-Defective Zr: A First-Principles Density Functional Theory Approach. *The Journal of Physical Chemistry C* **2023**, *127* (26), 12435-12443. DOI: 10.1021/acs.jpcc.3c01200.
(8) Tafen, D. N.; Paudel, H. P.; Duan, Y.; Redington, M. First-Principles Studies of Tritium Species Dissociability and Diffusivity Across the Interface of Nickel-Plated Zircaloy-4. In Conference: Conference Name: 8th Annual Tritium Science Technical Exchange Location: Richland, WA, United States Start Date: 9/26/2023 12:00:00 AM End Date: 9/27/2023 12:00:00 AM, United States; 2023.
(9) Senor, D. J. Recommendations for Tritium Science and Technology Research and Development in Support of the Tritium Readiness Campaign, TTP-7-084. DOI: 10.2172/1113608.
(10) Bair, J.; Asle Zaeem, M.; Tonks, M. A review on hydride precipitation in zirconium alloys. *J. Nucl. Mater.* **2015**, *466*, 12-20. DOI: https://doi.org/10.1016/j.jnucmat.2015.07.014. Motta, A. T.; Chen, L. Q. Hydride formation in zirconium alloys. *JOM* **2012**, *64* (12), 1403-1408, Article. DOI: 10.1007/s11837-012-0479-x.
(11) Kresse, G.; Furthmuller, J. Efficiency of ab-initio total energy calculations for metals and semiconductors using a plane-wave basis set. *Comp Mater Sci* **1996**, *6* (1), 15-50. DOI: Doi 10.1016/0927-0256(96)00008-0. Kresse, G.; Furthmüller, J. Efficient iterative schemes for ab initio total-energy calculations using a plane-wave basis set. *Physical Review B* **1996**, *54* (16), 11169-11186. DOI: 10.1103/PhysRevB.54.11169. Kresse, G.; Hafner, J. Ab initio molecular dynamics for liquid metals. *Physical Review B* **1993**, *47* (1), 558-561. DOI: 10.1103/PhysRevB.47.558.
(12) Blöchl, P. E. Projector augmented-wave method. *Phys Rev B* **1994**, *50* (24), 17953-17979. DOI: 10.1103/PhysRevB.50.17953. Kresse, G.; Joubert, D. From ultrasoft pseudopotentials to the projector augmented-wave method. *Phys Rev B* **1999**, *59* (3), 1758-1775. DOI: DOI 10.1103/PhysRevB.59.1758.
(13) Perdew, J. P.; Burke, K.; Ernzerhof, M. Generalized Gradient Approximation Made Simple. *Physical Review Letters* **1996**, *77* (18), 3865-3868. DOI: 10.1103/PhysRevLett.77.3865.
(14) Redingtona, M., Paudel, H. P., Tafen, D. N., Millere, D. P., Zurekb, E., Duan, Y., Tritium Adsorption on (100) and (001) Surfaces of Pure and Tin Defective Zirconium (under review). *Journal of Physical Chemistry C* **2024**.
(15) Henkelman, G.; Uberuaga, B. P.; Jónsson, H. A climbing image nudged elastic band method for finding saddle points and minimum energy paths. *The Journal of Chemical Physics* **2000**, *113* (22), 9901-9904. DOI: 10.1063/1.1329672 (acccessed 9/29/2023).
(16) Huang, L.-F.; Rondinelli, J. M. Electrochemical phase diagrams of Ni from ab initio simulations: role of exchange interactions on accuracy. *Journal of Physics: Condensed Matter* **2017**, *29* (47), 475501. DOI: 10.1088/1361-648X/aa9140. Jain, A.; Ong, S. P.; Hautier, G.; Chen, W.; Richards, W. D.; Dacek, S.; Cholia, S.; Gunter, D.; Skinner, D.; Ceder, G.; Persson, K. A. Commentary: The Materials Project: A materials genome approach to accelerating materials innovation. *APL Materials* **2013**, *1* (1). DOI: 10.1063/1.4812323 (acccessed 9/29/2023).
(17) Sahu, B. P.; Dutta, A.; Mitra, R. A combined electron microscopy and atom probe tomography study of the nanocrystalline Ni-Zr thin film. *Journal of Alloys and Compounds* **2020**, *844*, 156078. DOI: https://doi.org/10.1016/j.jallcom.2020.156078.
(18) Wang, N.; Li, C.; Du, Z.; Wang, F. Experimental study and thermodynamic re-assessment of the Ni–Zr system. *Calphad* **2007**, *31* (4), 413-421. DOI: https://doi.org/10.1016/j.calphad.2007.07.001.